RSC Advances

PAPER

View Article Online
View Journal | View Issue

Cite this: *RSC Adv.*, 2016, **6**, 77037

A biocompatible serine functionalized nanostructured zirconia based biosensing platform for non-invasive oral cancer detection†

Suveen Kumar, Jai Gopal Sharma, Sagar Maji and Bansi Dhar Malhotra*

We report results of studies relating to the fabrication of nontoxic, biocompatible serine functionalized nanostructured zirconia (serine/nZrO_2) for oral cancer detection. The hydrothermally synthesized ZrO_2 nanoparticles (~4.5 nm) have been characterized using X-ray diffraction (XRD) and transmission electron microscopy (TEM). The cytotoxicity studies of serine/nZrO_2 carried out using MTT assay on the HEK 293 human cell line reveal biocompatibility of the serine/nZrO_2. The serine functionalized nZrO_2 are electrophoretically deposited onto a hydrolysed indium tin oxide (ITO) coated glass electrode (serine/nZrO_2/ITO). Furthermore, monoclonal antibodies (anti-CYFRA-21-1) were covalently immobilized onto the serine/nZrO_2/ITO electrode and BSA was been used for blocking of the non-specific binding sites. The fabricated BSA/anti-CYFRA-21-1/serine/nZrO_2/ITO immunoelectrode was used for label free, non-invasive and efficient detection of an oral cancer biomarker (CYFRA-21-1). The electrochemical response studies of this immunoelectrode exihibited a wider linear detection range (0.01–29 ng mL^{-1}) with a remarkable detection limit (0.01 ng mL^{-1}) and a quick response time (6 min) for detection of the CYFRA-21-1 antigen. The results of validation studies conducted on the fabricated immunoelectrode (BSA/anti-CYFRA-21-1/serine/nZrO_2/ITO) using saliva samples of oral cancer patients indicate a good agreement with the results obtained *via* enzyme linked immunosorbent assay (ELISA).

Received 21st March 2016
Accepted 29th July 2016

DOI: 10.1039/c6ra07392a

www.rsc.org/advances

Introduction

There is increased interest towards the development of nontoxic, biocompatible and functionalized nanomaterials for biomedical applications.[1–7] To fabricate a biosensing platform, it is important that the surface of a desired nanomaterial should be modified with a functional group like –NH_2, –COOH, –OH *etc.*[8–11] To facilitate surface modification, an additional linker is required.[3] To date various linkers such as 3-aminopropyl triethoxy silane (APTES) and 3-mercaptopropyl triethoxy silane (MPTES) have been employed for this purpose.[3,10,12] Amongst these, APTES has been widely used as a linker to obtain a covalent bridge between a nanomaterial and a biomolecule.[12,13] However, the hazardousness of this linker molecule limits its use in biomedical applications.[14,15] It has been reported that the fumes of APTES can destroy mucous membranes of the upper respiratory tract, nerves system, liver and kidney.[12] Thus the use of APTES for functionalization of a matrix such as nanoparticles of metal, metal oxide, nanocomposite *etc.* may adversely affect the human health.[12] To overcome this limitation, a non-toxic linker may perhaps be advantageous both for functionalization of a nanomaterial and immobilization of desired biomolecules.

Amino acids are known to be nontoxic, organic compounds bearing amine (–NH_2) and carboxylic acid (–COOH) as functional groups along with a side chain that is known to be specific for each amino acid. About 500 different types of amino acids have been investigated till date and its side chain has been found to play an important role towards functionalization of nanomaterials.[16] Serine has been found to be a non-toxic, naturally occurring proteinogenic amino acid bearing –OH, –COOH and –NH_2 functional groups.[17,18] The hydroxyl group (–OH) in the serine molecule makes it a promising linker to obtain stable functionalization of a desired metal oxide and the presence of both –COOH and –NH_2 groups may provide efficient immobilization of desired biomolecules (antibodies, nucleic acid *etc.*).

Cancer is currently a leading cause of mortality worldwide and it is reported that in 2012 about 8.2 million deaths occurred due to cancer. Among the various cancers, oral cancer is the 6th most common death causing disease in the world.[9] It occurs on the floor of mouth, lips, sinuses, cheeks, throat *etc.*[19] Certain genes such as P16, APC and p53 get altered resulting in uncontrolled growth of cells leading to oral cancer.[20] At an early stage, most of patients do not exhibit any symptoms. However, with the passage of time, symptoms such as mouth ulcer, loss of teeth and hoarse voice appear. The conventional techniques

Nanobioelectronics Laboratory, Department of Biotechnology, Delhi Technological University, Delhi 110042, India. E-mail: bansi.malhotra@gmail.com

† Electronic supplementary information (ESI) available. See DOI: 10.1039/c6ra07392a

such as biopsy, brush cytology, laser-capture micro dissection, toluidine blue staining and tissue reflectance are being currently used for the diagnosis of oral cancer.[21–23] Most of these techniques are invasive, expensive, highly painful and require expertise for sample collection as well as analysis. There is an urgent need for the availability of a non-invasive biosensor for detection of oral cancer at an early stage.

For non-invasive detection; saliva, urine, sweat and tears can be used as analytical samples that are known to comprise of various biomarkers.[24] In the saliva of oral cancer patients, many biomarkers such as interlukin-1 (IL-1), interlukin-6 (IL-6), interlukin-8 (IL-8), endothelin-1 (ET-1) protein and mRNA, has-miR-200a and CYFRA-21-1 are secreted.[25–28] Efforts have been made to fabricate non-invasive biosensor based on salivary biomarker for oral cancer detection. Li *et al.* used salivary transcriptome (RNA) for detection of oral cancer, wherein salivary RNA was isolated from saliva supernatant and amplified using T7 RNA polymerase *via* quantitative polymerase chain reaction (qPCR).[29] Wang *et al.* developed a magnetic controllable electrochemical RNA biosensor for ultra sensitive and specific detection of salivary miRNA. They used magnetic controlled gold electrode and magnetic beads based enzymatic catalysis amplification for miRNA detection.[30] Yang *et al.* reported electrochemical biosensor for detection of trace level of salivary IL-8 protein.[31] Choudhary *et al.* developed salivary CD 59 biomarker based immunosensor for oral cancer detection.[32] It may be noted that these biomarkers are secreted at very low concentration ($\sim$pg mL^{-1}) necessitating detection by tagging of biomolecules making the whole process highly complex.

CYFRA-21-1 is an acidic protein salivary biomarker which represents a fragment of 40 kD of cytokeratin 19.[33] The physiological range of CYFRA-21-1 secreted in human saliva is in the range, 0–18 ng mL^{-1}. In a normal person its concentration is up to 3.8 ng mL^{-1}. However, in oral cancer patients its concentration increases to 17.46 $\pm$ 1.46 ng mL^{-1}. The specific cut-off concentration (3.8 ng mL^{-1}) can be used to classify cancerous from non-cancerous subjects.[27,28] Efforts have recently been made for the diagnosis of oral cancer *via* CYFRA-21-1 detection. Kumar *et al.* reported fabrication of an electrochemical biosensor based on APTES functionalized nanomaterials that does not cover the whole physiological range (*i.e.* 0 to 17.46 $\pm$ 1.46 ng mL^{-1}) of CYFRA-21-1 secreted in saliva of oral cancer patients.[8,9]

We report results of the studies relating to application of functionalized metal oxide ($nZrO_2$) with non-toxic serine molecules for fabrication of the biosensing platform for non-invasive oral cancer biomarker (CYFRA-21-1) detection. This fabricated immunosensor covers the entire physiological range of CYFRA-21-1 biomarker secreted in saliva samples with improved biosensing characteristics. The obtained results have been validated *via* gold standard technique *i.e.* ELISA for protein molecules.

Materials and methods

Chemicals

Zirconium ethoxide, serine, 3-(4,5-dimethylthiazol-2-yl)-2,5-diphenyltetrazolium bromide (MTT) and 1-(3-(dimethyl-amino)-propyl)-3-ethylcarbodiimide hydrochloride (EDC) were purchased from Sigma Aldrich. Sodium hydroxide pellets, cetyltrimethylammonium bromide (CTAB), sodium monophosphate, sodium diphosphatedihydrate, *N*-hydroxy-sulfosuccinimide (NHS), sodium chloride, potassium ferricyanide and potassium ferrocyanide were procured from Fisher Scientific. All chemicals were of analytical grade and were used without any further purification. Fresh phosphate buffer saline (PBS) solution of pH 7.0 was prepared using sodium monophosphate (0.05 mol L^{-1}) and sodium diphosphatedihydrate (0.05 mol L^{-1}) using Milli-Q water having resistivity of 18 MΩ cm and stored at 4 °C. The HEK 293 cell line was purchased from National Centre for Cell Science (NCCS, Pune, India). The CYFRA-21-1 and anti-CYFRA-21-1 were obtained from Ray Biotech, Inc., India. These biomolecules were further diluted by using PBS buffer of pH 7.0. CYFRA-21-1 ELISA Kit was purchased from KinesisDX, USA.

Instrumentation

Phase and crystallinity of synthesized $nZrO_2$ were determined using X-ray diffraction (XRD) [Bruker D-8 Advance] measurements. For this purpose, a monochromatic X-ray beam with Cu-Kα radiation (λ = 1.5406 Å) was used. Fourier transform infrared spectroscopy (FT-IR, Perkin-Elmer, model 2000) studies were conducted to investigate the functionalization of $nZrO_2$ with serine and protein immobilization on serine/$nZrO_2$/ITO electrode. For morphological studies, we performed transmission electron microscopy (TEM) and high resolution transmission electron microscopy (HR-TEM) (Tecnai G2 20 twin microscope with accelerating voltage of 200 kV) studies. To investigate the hydrophilic/hydrophobic behaviour of ITO, APTES/$nZrO_2$/ITO, serine/$nZrO_2$/ITO and anti-CYFRA-21-1/serine/$nZrO_2$/ITO electrodes, the contact angle studies were carried out using Data Physics OCA15EC instrument. Electrochemical studies were done by differential pulse voltammetry (DPV) and cyclic voltammetry (CV) techniques in PBS buffer using an Autolab Potentiostat (Netherlands).

Preparation and functionalization of zirconia nanoparticles with serine

The solutions containing 0.1 M zirconium ethoxide, 1 M sodium hydroxide and 0.1 M of CTAB in 50 mL of deionized water were separately prepared. 10 mL of CTAB solution was added to zirconium ethoxide solution and constantly stirred (300 rpm) at 40 °C for 2 h. Further, 1 mL of sodium hydroxide solution was added drop-wise in the above reaction mixture and kept under constant stirring for another 2 h. Further, the prepared solution was kept in the water bath for 1 h at 60 °C after which it was immediately kept under running tap water. Next, the solution was transferred to a Teflon vessel comprising of hydrothermal pressure assembly. This assembly was further kept in an oven at 170 °C for 17 h. After cooling, the precipitate obtained from the reaction was washed with deionized water through the centrifugation process until pH of the solution became neutral. Subsequently, the obtained slurry was dried at 80 °C over night and annealed at 400 °C for 3 h. The obtained

product was crushed into fine powder for further characterization.

For functionalization of the synthesized zirconia nanoparticles, serine was used. A dispersed suspension of 100 mg of $nZrO_2$ in 25 mL of isopropanol was prepared after which 20 mg of serine was added. 10 mL of deionized water was later added to the above mixture and kept at room temperature with constant stirring (300 rpm) for 48 h. To remove the unbound serine molecules, the suspension was filtered using Whatman paper and washed thoroughly with deionized water. Thus obtained slurry was dried at 100 °C for 7 h. The product was finely crushed and stored in a dry place until further use.

Cell proliferation study

The cytotoxicity of serine/$nZrO_2$ and APTES/$nZrO_2$ was evaluated *in vitro* on HEK 293 cell line by MTT colorimetric assay. This assay involves reduction of yellow colored MTT dye into purple colored formazan product by mitochondrial succinate dehydrogenase enzyme in live cells. The obtained formazan crystals were further solubilized in a buffer and the intensity of the color was measured spectrophotometrically at 540 nm on an ELISA plate reader. The cells were seeded in a 96 well plate at initial cell density of 10^5 cells per well and incubated at 37 °C in a humidified 5% CO_2 atmosphere. When the cells attained 70% confluence, both serine/$nZrO_2$ and APTES/$nZrO_2$ were added to the wells at concentration of 10 μg mL^{-1} to 250 μg mL^{-1}. The cells were incubated for 48 h in CO_2 incubator. After 48 h of incubation MTT assay was carried out, briefly 200 μL of MTT solution (0.5 mg mL^{-1} in DMEM) was added to each well. The cells were incubated for 2 h. After 2 h the supernatant was aspirated and the buffer (100 μL isopropanol containing 0.06 M HCl and 0.5% SDS) was added to each well to solubilize the formazan crystals. The absorbance of this colored solution was measured at 540 nm on an ELISA plate reader (MRX Dynatech laboratory, US). Untreated cells were taken as control with 100% viability and wells with MTT reagent without cells were used as blank to calibrate the spectrophotometer to zero absorbance. The relative cell viability (%) compared to control cells was calculated by $[abs]_{sample}/[abs]_{control} \times 100$. All the experiments were carried out in triplicate.

Fabrication of biosensing platform

We prepared a solution containing 2 mg mL^{-1} serine functionalized zirconia nanoparticles (serine/$nZrO_2$) by dispersing it in acetonitrile with mild ultrasonication. Thin film of serine/$nZrO_2$ was electrophoretically deposited onto pre-hydrolyzed ITO coated glass electrode using a two electrodes system, where ITO coated glass electrode worked as an anode and platinum wire as cathode, placed parallelly at a distance of 1 cm in a glass cell. Prior to application of the optimized DC potential (*i.e.* 50 V for 35 s), 50 μL of magnesium nitrate solution (10^{-5} M) was added to get surface charge on serine/$nZrO_2$. The serine/$nZrO_2$ film deposited on to ITO was washed with PBS buffer to remove any unbound serine/$nZrO_2$ molecules.

The solution comprising of 15 μL of anti-CYFRA-21-1 (50 μg mL^{-1}), 7.5 μL of EDC (0.4 M) and 7.5 μL of NHS (0.1 M) was prepared. 30 μL of this solution was uniformly spread onto serine/$nZrO_2$/ITO electrode by drop-casting and kept in a humid chamber at room temperature (25 °C) for the formation of covalent bond between –COOH group present on Fc region of anti-CYFRA-21-1 and $-NH_2$ group of serine molecules. The prepared immunoelectrode (anti-CYFRA-21-1/serine/$nZrO_2$/ITO) was washed with PBS to remove any unbound antibodies. Lastly, 10 μL of BSA (2 mg dL^{-1}) was used for blocking non-specific active sites of the immunoelectrode. The fabricated BSA/anti-CYFRA-21-1/serine/$nZrO_2$/ITO immunoelectrode was washed with PBS and stored at 4 °C until further use.

Collection of saliva samples of oral cancer patients

The saliva samples of oral cancer patients were obtained after ethical approval by the Institutional Review Board of Rajiv Gandhi Cancer Institute and Research Centre (RGCIRC) Delhi (India) and Institutional Ethical and Biosafety Committee, DTU. We also took written consent of patients prior to collection of the saliva samples. Thereafter we took saliva samples of seven oral cancer patients from RGCIRC. We collected un-stimulated saliva samples after rinsing the mouths of patients with 5 mL deionized water and expectorated these into sterilized tube. These samples were centrifuged at 2800 rcf (25 °C) for 30 min. The supernatant was collected in sterilized Eppendorf and stored at −20 °C till further usage.[28]

Results and discussion

X-ray diffraction (XRD) and transmission electron microscopic (TEM) studies

Synthesized whitish nano powder was characterized through XRD technique in the range of 2θ angle from 20 to 70°. The peaks obtained at 24.5°, 28.2°, 41.5°, 45.2°, 50.5°, 54.2°, 57.0°, and 66.1° indicate the presence of monoclinic phase of zirconia molecules in plane of (011), (−111), (−121), (−202), (−221), (003), (−113) and (−132) respectively (JCPDS no. 37–1484). The peaks seen at 30.3°, 34.9°, 60.1° and 63.0° reveal the presence of tetragonal phase of zirconia molecules in plane of (101), (002), (211) and (202) respectively (JCPDS no. 80–2155). These results revealed the synthesis of mixed phase (monoclinic and tetragonal) of zirconia nanoparticles (Fig. 1a).

The average crystallite size "*D*" of synthesized nanoparticles was estimated to be ~4.5 nm using the Debye–Scherrer equation (eqn (1))

$$D = 0.9\lambda/\beta \cos\theta \quad (1)$$

where $\lambda = 1.540$ Å is the wavelength of the target Cu-Kα, θ is the Bragg's diffraction angle, and β is the full width at half maximum (FWHM) of the diffraction peak.

The morphology of the synthesized zirconia nanoparticles was investigated *via* transmission electron microscopy (TEM) (Fig. 1b and c). These zirconia nanoparticles were dispersed in ethanol and drop cast on a carbon coated copper TEM grid and dried at room temperature. The TEM image indicates formation of the uniform spherical shape of nanoparticles. Further, the

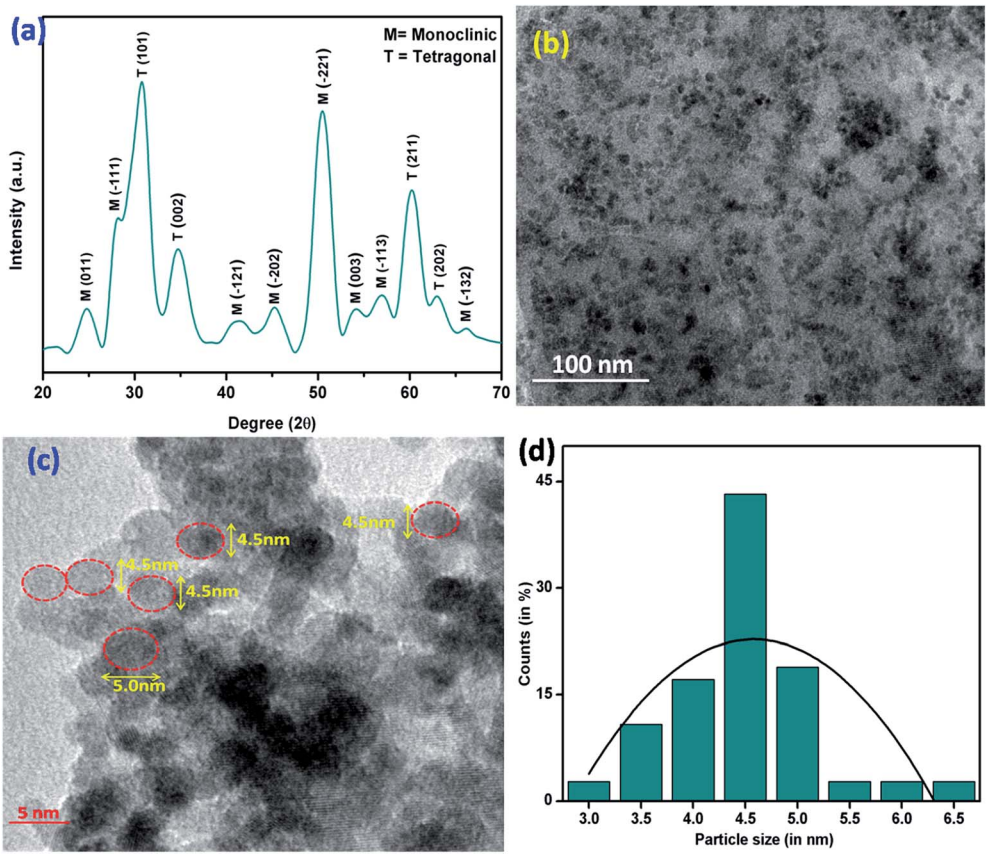

Fig. 1 (a) XRD pattern (b) TEM (c) HR-TEM images and (d) particle size distribution of zirconia nanoparticles.

particle size was investigated by histogram fitted with the Gaussian function and was calculated to be ~4.5 nm (Fig. 1d).

Fourier transform infrared (FT-IR) spectroscopic studies

Fig. S1† shows FT-IR spectra of the serine amino acid. The peaks observed in between 1010 to 1300 cm^{-1} are due to presence of C–O bond of carboxyl group. A broad peak obtained in 1520 to 1680 cm^{-1} range is due to bending of N–H bond present as primary amine in serine that helps in the formation of covalent bond with carboxylic groups of biomolecules. Peak obtained at 1465 cm^{-1} represents C–H bond. The broad peak obtained in between 2780 to 3680 cm^{-1} is due to cumulative effect of the bonds such as C–H stretching, free –OH group present in the serine molecules.[34] Fig. 2 shows FT-IR spectra of the zirconia nanoparticles (curve a) and serine functionalized zirconia nanoparticles (serine/$nZrO_2$, curve b). In both curve a and curve b, the characteristic peak present at 550 cm^{-1} is due to symmetric stretching of the Zr–O bond.[35] Furthermore, in curve b, the band seen in the region, 1010 to 1300 cm^{-1} is due to C–O of carboxyl group. The 1590 cm^{-1} is due to bending of the N–H bond present on the serine molecules indicating successful functionalization of zirconia nanoparticles *via* serine molecules.[36] The intensity of the peak found at 3400 cm^{-1} is due to cumulative effect of N–H and O–H groups present in the serine molecules.[36] And the extra peaks found at 1470 and 2980 cm^{-1} are due to presence of CH_2 bending and C–H stretching vibrations of serine molecules, respectively.[36]

Cytotoxicity studies

The cytotoxicity of a nanomaterial plays an important role in the fabrication of biosensing platform. To investigate the toxicity of functionalized nanostructured zirconia (serine/$nZrO_2$ and

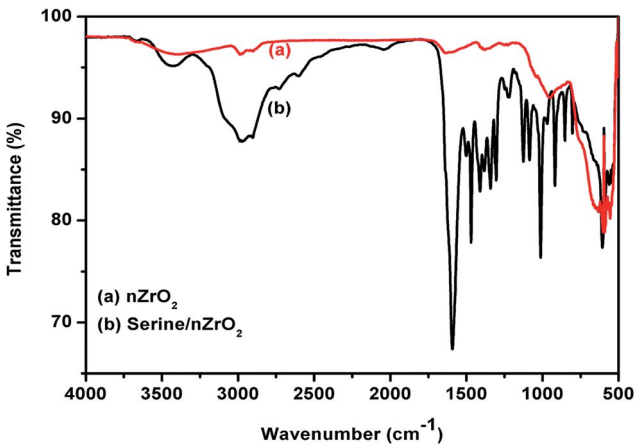

Fig. 2 FTIR spectra of (a) $nZrO_2$ nanoparticles and (b) serine functionalized $nZrO_2$ nanoparticles (serine/$nZrO_2$).

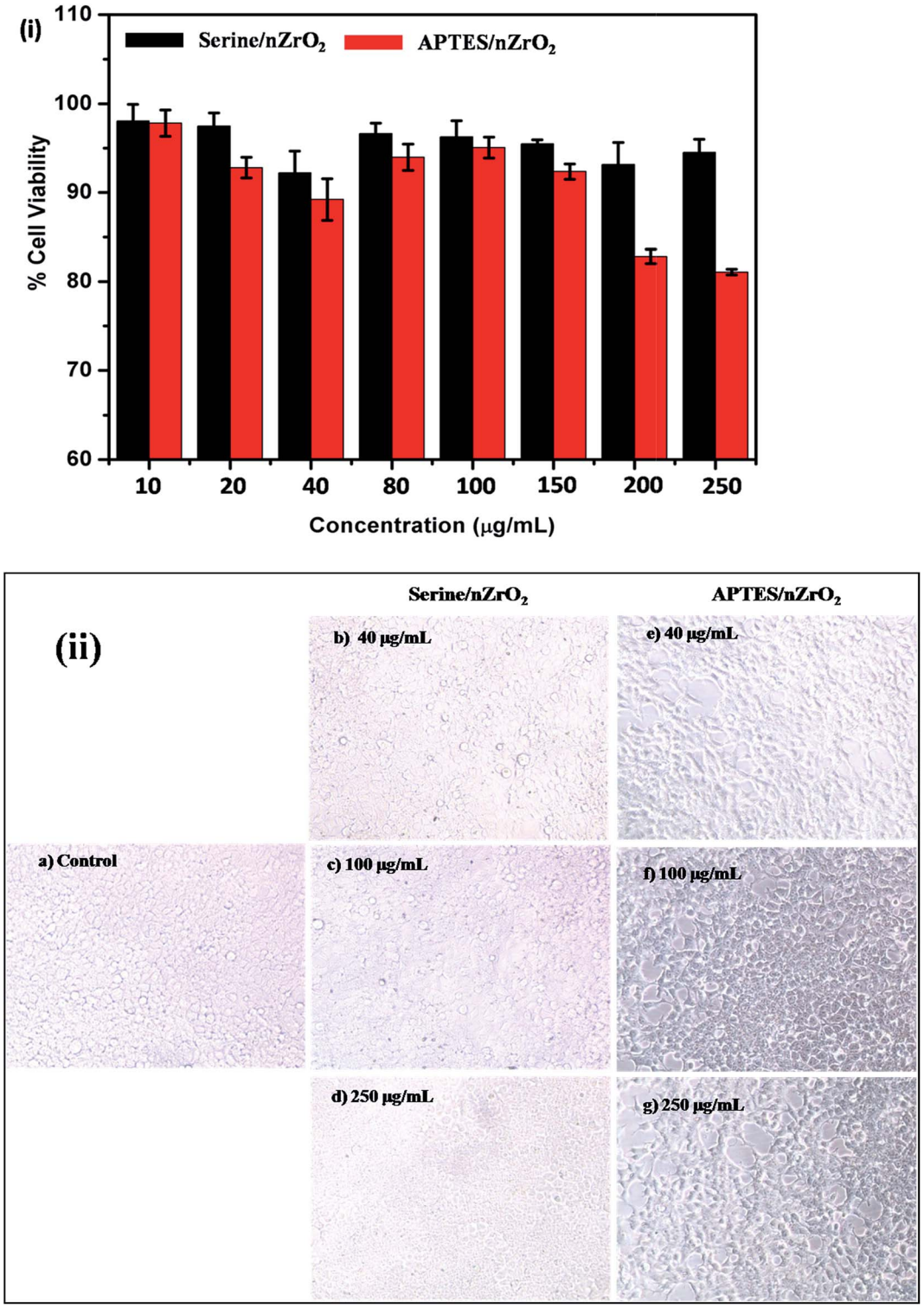

Fig. 3 (i) % cell viability and (ii) morphology of HEK 293 cell line with different concentration of serine/$nZrO_2$ and APTES/$nZrO_2$.

APTES/$nZrO_2$), MTT assay was conducted on HEK 293 cell lines. The results of MTT assay reveal that serine/$nZrO_2$ does not exhibit any significant cytotoxicity on HEK 293 cell line in the concentration range 10 to 250 μg mL^{-1}. Fig. 3(i) shows the comparative cell viability on samples of serine/$nZrO_2$ and APTES/$nZrO_2$. The results indicate increased detrimental effect of the APTES functionalized zirconia beyond 10 μg mL^{-1} on cell viability where as in the case of the serine functionalized zirconia the cell viability was found to be more than 95% up to 250 μg mL^{-1} concentration. Fig. 3(ii) depicts the cell

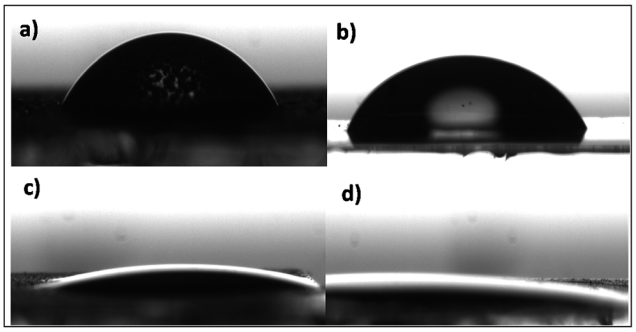

Fig. 4 Contact angle measurements of (a) ITO (b) APTES/$nZrO_2$/ITO (c) serine/$nZrO_2$/ITO and (d) anti-CYFRA-21-1/serine/$nZrO_2$/ITO electrodes.

morphology of HEK 293 cell line on exposure to different concentrations. It is observed that cell morphology remains unchanged for the serine/$nZrO_2$ film with respect to control cell line. On the other hand, cells degrade progressively in case of APTES/$nZrO_2$. These results reveal that serine/$nZrO_2$ exhibited higher biocompatibility.

Contact angle studies

The value of contact (CA) of hydrolyzed ITO electrode was determined to be 66.22° indicating highly hydrophobic nature of ITO (Fig. 4a). The CA of APTES/$nZrO_2$/ITO was measured as 63.13° (Fig. 4b) indicating slightly hydrophilic nature with respect to the ITO. The CA of electrophoretically deposited serine functionalised zirconia nanoparticles (serine/$nZrO_2$/ITO) found out to be 18.97° indicated rapid change in the hydrophilic behaviour (Fig. 4c) as compared to that of the APTES/$nZrO_2$/ITO electrode. This improved hydrophilic behaviour of serine/$nZrO_2$/ITO electrode provided highly favourable microenvironment for anti-CYFRA-21-1 immobilization. After immobilization of anti-CYFRA-21-1 onto serine/$nZrO_2$/ITO (Fig. 4d) electrode, the CA value decreased to 14.92° indicating further increase in hydrophilic nature of the anti-CYFRA-21-1/serine/$nZrO_2$/ITO immunoelectrode due to the covalent attachment of the anti-CYFRA-21-1 on serine/$nZrO_2$/ITO.

Electrochemical studies

For electrochemical studies, the phosphate buffer saline (PBS) containing 5 mM $[Fe(CN)_6]^{3-/4-}$ was used as an electrolyte. The effect of pH on the electrochemical response of BSA/anti-CYFRA-21-1/serine/$nZrO_2$/ITO immunoelectrodes was investigated using cyclic voltammetry (CV) at a scan rate 50 mV s^{-1}. The maximum peak current was obtained at pH 7.0 (Fig. S2†). This could perhaps be attributed to the biological entities that are present in their natural form at neutral pH. However, in case of acidic or basic medium they perhaps got denatured due to the interaction of H^+ or OH^- ions on the amino acid sequence of antibodies.[37]

Fig. S3† shows results of the CV studies conducted onto ITO, serine/$nZrO_2$/ITO, anti-CYFRA-21-1/serine/$nZrO_2$/ITO, and BSA/anti-CYFRA-21-1/serine/$nZrO_2$/ITO electrode, respectively in PBS solution (50 mM, pH 7.0, 0.9% NaCl) containing 5 mM of $[Fe(CN)_6]^{3-/4-}$ at a scan rate of 50 mV s^{-1} in the potential range, −0.8 V to 0.8 V. The magnitude of peak current obtained for serine/$nZrO_2$/ITO electrode (0.049 mA) was lower than that of the bare ITO electrode (0.052 mA), indicating decreased electron transfer between solution and the serine/$nZrO_2$/ITO interface. Further, the peak current measured for anti-CYFRA-21-1/serine/$nZrO_2$/ITO immunoelectrode was 0.051 mA. Increase in peak current of the anti-CYFRA-21-1/serine/$nZrO_2$/ITO immunoelectrode could be due to serine/$nZrO_2$/ITO electrode that acted as a mediator on the electrode surface. This perhaps led to significant decrease in the electron tunneling distance between the antibodies and the electrode resulting in higher peak current. Besides this, the electrostatic interaction between the free sites of the antibodies ($-NH_2$ terminal) and the redox species perhaps resulted in fast electron diffusion toward the immunoelectrode.[38] BSA was used to prevent non-specific binding site of the fabricated immunoelectrode. After BSA immobilization, the magnitude of peak current decreased to 0.034 mA due to non-specific adsorption of BSA onto the exposed serine/$nZrO_2$ sites of the anti-CYFRA-21-1/serine/$nZrO_2$/ITO immunoelectrode.

Interfacial kinetics of the serine/$nZrO_2$/ITO and BSA/anti-CYFRA-21-1/serine/$nZrO_2$/ITO electrodes surface was investigated using scan rate, varying from 40 to 150 mV s^{-1} (Fig. S4 and S5†). The magnitudes of anodic (I_{pa}) and cathodic (I_{pc}) peak currents increased linearly indicating that the electrochemical reaction was a diffusion control process.[39] The slopes and intercepts could be determined using eqn (2)–(5).

$$I_{pc(serine/nZrO_2/ITO)} = [54.46\ \mu A\ s\ mV^{-1} \times (\text{scan rate } [mV\ s^{-1}])^{1/2}] + 113.85\ \mu A,\ R^2 = 0.999 \quad (2)$$

$$I_{pa(serine/nZrO_2/ITO)} = -[38.83\ \mu A\ s\ mV^{-1} \times (\text{scan rate } [mV\ s^{-1}])^{1/2}] - 146.61\ \mu A,\ R^2 = 0.999 \quad (3)$$

$$I_{pc(BSA/anti\text{-}CYFRA\text{-}21\text{-}1/serine/nZrO_2/ITO)} = [35.77\ \mu A\ s\ mV^{-1} \times (\text{scan rate } [mV\ s^{-1}])^{1/2}] + 82.91\ \mu A,\ R^2 = 0.999 \quad (4)$$

$$I_{pa(BSA/anti\text{-}CYFRA\text{-}21\text{-}1/serine/nZrO_2/ITO)} = -[28.84\ \mu A\ s\ mV^{-1} \times (\text{scan rate } [mV\ s^{-1}])^{1/2}] - 71.71\ \mu A,\ R^2 = 0.999 \quad (5)$$

The results of scan rate studies of both BSA/anti-CYFRA-21-1/serine/$nZrO_2$/ITO and serine/$nZrO_2$/ITO electrodes revealed that the oxidation peaks shifted more towards the positive potential and similarly reduction peak shifted toward more negative potential. The difference of cathodic peak potential (E_{pc}) and anodic peak potential (E_{pa}) showed a linear relationship with increasing scan rate as given by eqn (6) and (7) (inset a and b of Fig. S4 and S5†) indicating a facile electron transfer from the medium to electrode.[38]

$$\Delta E_p(V)_{serine/nZrO_2/ITO} = [0.016\ V\ s\ mV^{-1} \times (\text{scan rate } [mV\ s^{-1}])^{1/2}] + 0.109\ V,\ R^2 = 0.999 \quad (6)$$

$$\Delta E_p(V)_{BSA/anti\text{-}CYFRA\text{-}21\text{-}1/serine/nZrO_2/ITO} = [0.031\ V\ s\ mV^{-1} \times (\text{scan rate } [mV\ s^{-1}])^{1/2}] + 0.164\ V,\ R^2 = 0.999 \quad (7)$$

Response time studies

To determine the incubation time required to interact CYFRA-21-1 with BSA/anti-CYFRA-21-1/serine/$nZrO_2$/ITO immunoelectrodes we conducted response time studies at a regular time interval of up to 30 minutes (Fig. S6†) using DPV. We observed that current response increased from 0 to 6 minutes after which it became nearly constant. This result showed that about 6 minutes were required for complete interaction between CYFRA-21-1 with BSA/anti-CYFRA-21-1/serine/$nZrO_2$/ITO immunoelectrode. For further electrochemical studies we gave 6 minutes for incubation prior to each measurement.

Response studies

The electrochemical response of the BSA/anti-CYFRA-21-1/serine/$nZrO_2$/ITO immunoelectrode was measured as a function of CYFRA-21-1 concentration (0.01–29 ng mL^{-1}) with incubation time of about 6 minutes. Three electrodes system was used for this purpose, wherein the immunoelectrode worked as the working electrode, Ag/AgCl as reference electrode and platinum wire as counter electrode in phosphate buffer saline (PBS, 50 mM, pH 6.0 and 0.9% NaCl) containing 5 mM $[Fe(CN)_6]^{3-/4-}$ as a mediator. It was found that peak current increased on interaction of the antigens with antibodies at the electrode/electrolyte interface (Fig. 5). The sequence of CYFRA-21-1 protein (Accession: AAF27048.1, cytokeratin 19 fragments, *Homo sapiens*) is known to contain 14 residues of tyrosine (Y) molecules. During an electrochemical reaction, these tyrosine molecules undergo oxidation and release electrons resulting in increased peak current.[40,41] The increased concentration of amino acids due to increased concentration of CYFRA-21-1 antigen is likely to result in enhanced antigen–antibody interaction onto serine/$nZrO_2$/ITO electrode leading to increased peak current.[9] The plot between peak current and CYFRA-21-1 concentration shows linearity between 0.01 to 29 ng mL^{-1} with regression coefficient of 0.997 and follows eqn (8):

$$I_p = [29.44\ mA\ mL\ ng^{-1}) \times (\text{conc. of CYFRA-21-1 } (ng\ mL^{-1}))] + 0.042\ mA,\ R^2 = 0.997 \quad (8)$$

The sensitivity of the BSA/anti-CYFRA-21-1/serine/$nZrO_2$/ITO immunoelectrode was found to be 0.295 μA mL ng^{-1}. The proposed biosensor shows enhanced linear detection range (0.01 to 29 ng mL^{-1}) as compared to the previously proposed biosensor. Increase in linear detection range may be due to increased loading of anti-CYFRA-21-1 on the serine/$nZrO_2$/ITO

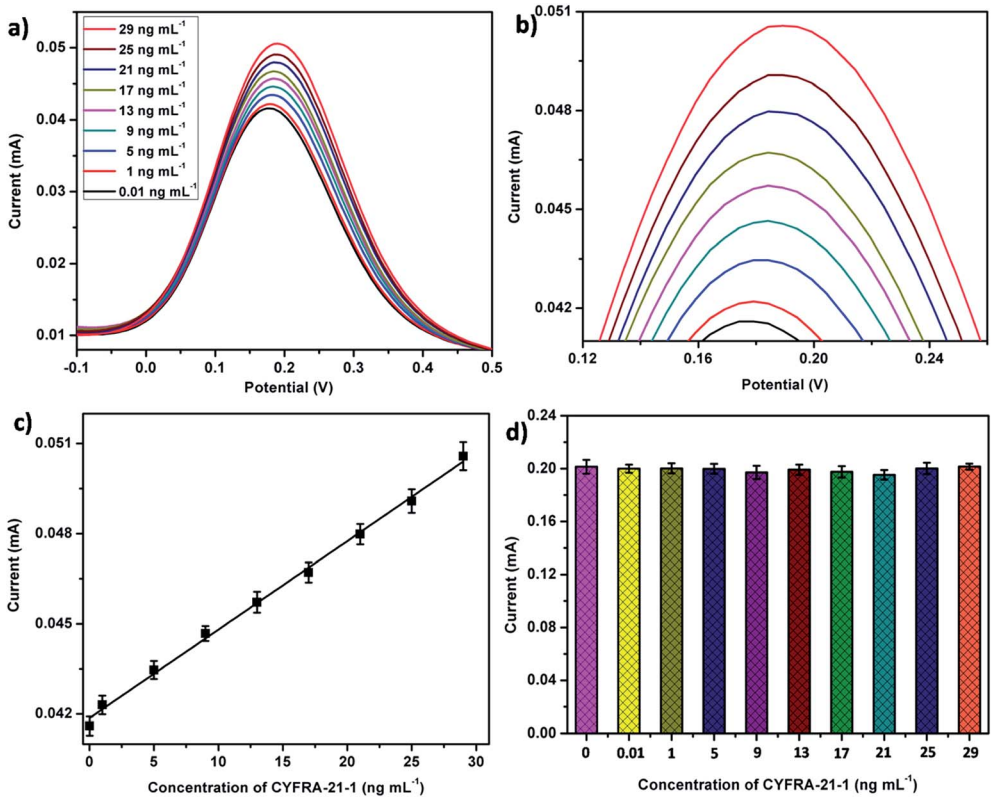

Fig. 5 (a) DPV response studies of BSA/anti-CYFRA-21-1/serine/$nZrO_2$/ITO immunoelectrode as a function of CYFRA-21-1 concentration (0.01–29 ng mL^{-1}), (b) magnified view of peak current response, (c) calibration curve between the magnitude of peak current and concentration of CYFRA-21-1 (ng mL^{-1}) and (d) A control experiment of serine/nZrO2/ITO electrode as a function of CYFRA-21-1 concentration (0.01–29 ng mL^{-1}).

Table 1 Characteristics of the various detection techniques used for oral cancer detection

Method	Detection technique	Invasive/ non-invasive	Label	Sample	Biomarker	Platform	Concentration range of biomarker	Linear detection range	Response time	Lower detection limit	Reference
Cytopathology	Staining	Invasive	—	Cells	—	—	—	—	1 week	—	23
Biopsy	Cell culture	Invasive	—	Tissue	—	—	—	—	2–3 weeks	—	22
Visualization adjuncts	Staining	Invasive	—	Tissue	—	—	—		1 week	—	22
Biosensor	Amperometric	Invasive	Yes	Serum	IL-6 (protein)	—	≤6 pg mL^{-1} to ≥20 pg mL^{-1}	0.5–30 pg mL^{-1}	—	—	25
	DPV	Invasive	Yes	Serum	IL-6 (protein)	—	<6 pg mL^{-1} to >20 pg mL^{-1}	0.002–20 ng mL^{-1}	—	—	42
	CV	Non-invasive	Yes	Saliva	Has-miR-200a (mi-RNA)	—	—	1 aM to 10 fM	—	—	30
	CV	Non-invasive	No	Saliva	CYFRA-21-1 (protein)	BSA/anti-CYFRA-21-1/ APTES/ZrO_2/ITO	0–18 ng mL^{-1}	2–16 ng mL^{-1}	20 min	0.08 ng mL^{-1}	8
	CV	Non-invasive	No	Saliva	CYFRA-21-1 (protein)	BSA/anti-CYFRA-21-1/ APTES/*n*HfO_2/ITO	0–18 ng mL^{-1}	2–18 ng mL^{-1}	15 min	0.21 ng mL^{-1}	43
	DPV	Non-invasive	No	Saliva	CYFRA-21-1 (protein)	BSA/anti-CYFRA-21-1/ APTES/ZrO_2-RGO/ITO	0–18 ng mL^{-1}	2–22 ng mL^{-1}	16 min	0.122 ng mL^{-1}	9
	DPV	Non-invasive	No	Saliva	CYFRA-21-1 (protein)	BSA/anti-CYFRA-21-1/ serine/nZrO_2/ITO	0–18 ng mL^{-1}	0.01–29 ng mL^{-1}	6 min	0.01 ng mL^{-1}	Present work

electrode as compared to that of the APTES/nZrO_2/ITO electrode (Table 1). Scheme S1† shows the schematic of serine/nZrO_2/ITO with APTES/nZrO_2/ITO indicating that the average bearing of anti-CYFRA-21-1 by serine/nZrO_2/ITO electrode is more (more than six times) as compared to that of APTES/nZrO_2/ITO electrode. These results reveal that the serine/nZrO_2/ITO can hold more number of biomolecules of anti-CYFRA-21-resulting in increased linearity.

A control experiment was carried to investigate the electrochemical response of serine/nZrO_2/ITO electrode as a function of CYFRA-21-1 concentration. We did not observe (Fig. 5d) any significant electrochemical response with increased CYFRA-21-1 concentration. The results indicate that the serine/nZrO_2/ITO electrode surface did not interact with the antigen molecules revealing the electrochemical response remained unchanged.

Interference studies

A number of biomolecules including sodium carboxymethyl cellulose (NaCM) [10 mg mL^{-1}], glucose [7 mg mL^{-1}], potassium chloride (KCl) [8.38 mM], calcium chloride ($CaCl_2$) [1.13 mM], sodium chloride (NaCl) [20 mM], carcinoembroyonic antigen (CEA) [4–16 ng mL^{-1}], *etc.* are known to be present in human saliva of oral cancer patients. To investigate its effect on the electrochemical response of BSA/anti-CYFRA-21-1/serine/nZrO_2/ITO immunoelectrodes, we conducted interferents studies (Fig. S7†). Firstly, we measured the electrochemical response of BSA/anti-CYFRA-21-1/serine/nZrO_2/ITO immunoelectrode towards the CYFRA-21-1 (0.01 ng mL^{-1}) using differential pulse voltammetry (DPV). Thereafter we added NaCM, glucose, KCl, $CaCl_2$, NaCl and CEA one by one in same solution containing CYFRA-21-1 and measured the response *via* DPV. We did not observe any significant changes in the peak current (% RSD < 1%) indicating that the fabricated immunoelectrode showed high selectivity towards the CYFRA-21-1 biomarker.

To investigate the cumulative effect of analytes/ions and effect of addition of different amount of saliva sample we prepared artificial saliva samples, we took different quantities of artificial saliva and observed the peak current response by BSA/anti-CYFRA-21-1/serine/nZrO_2/ITO immunoelectrode (Fig. S8†). It was found that DPV peak response current remained unchanged up to 1000 μL of artificial saliva after which it decreased. This result revealed that presence of analytes as well as ions did not affect the peak current response up to 1000 μL. For the electrochemical response studies we took only 20 μL of each sample so that no false current was generated.

Real sample analysis

We collected and processed the saliva samples of seven oral cancer patients. Double-antibody sandwich ELISA technique was used to quantify the concentration of CYFRA-21-1 protein biomarker in the processed saliva samples. In the double-antibody sandwich ELISA, anti-CYFRA-21-1 precoated microtiter 96 wells plate were used. After following all the steps, colorimetric reaction occurred and the absorbance was recorded at 450 nm in ELISA plate reader.

A series of saliva samples containing CYFRA-21-1 concentration were obtained by ELISA (Table S1†) to validate the electrochemical response of the fabricated biosensor. It was found that a reasonable correlation existed between magnitude of the CV current response of the fabricated immunoelectrode in the presence of (a) CYFRA-21-1 concentration in saliva samples determined by ELISA and (b) standard concentration of CYFRA-21-1 (Table S1, ESI†). The results obtained showed average %RSD (relative standard deviation) to be 4.4%, indicating high accuracy of the fabricated biosensor for CYFRA-21-1 biomarker detection.

The sensing characteristics of proposed immunosensor are summarized in Table 1 along with those reported in the literature.

Reproducibility and shelf life studies

Five different BSA/anti-CYFRA-21-1/serine/nZrO_2/ITO immunoelectrodes were fabricated and used for the reproducibility studies. DPV technique was used to study the reproducibility under similar set of conditions with concentration of CYFRA-21-1 (0.01 ng mL^{-1}). The immunoelectrodes exhibited high reproducibility with average standard deviation of up to 1.962% (Fig. S9†).

The shelf life study of BSA/anti-CYFRA-21-1/serine/nZrO_2/ITO immunoelectrode was investigated by DPV at regular intervals for up to 60 days. Immunoelectrode was stored at 4 °C in dark condition when not in use. It was observed that the fabricated immunoelectrode exhibited 95% of peak current response up to 45 days after which the peak current decreased and reached 80% (Fig. S10†) indicating that the fabricated immunoelectrode showed stability of up to 45 days in controlled environmental conditions.

Conclusions

We have proposed a new biosensing platform based on non-toxic serine amino acid as linker molecules for the functionalization of nZrO_2 for fabrication of an efficient, label-free and non-invasive biosensing platform for oral cancer biomarker (CYFRA-21-1) detection. The nanostructured zirconia (~4.5 nm) synthesized *via* one step low temperature hydrothermal process and further serine molecules was used for functionalization through simple chemical process. The serine functionalized ZrO_2 (serine/nZrO_2) was further electrophoretically deposited onto ITO coated glass electrode at 50 V for 35 s. Further, the serine/nZrO_2/ITO film was biofunctionalized with anti-CYFRA-21-1 *via* EDC–NHS covalent surface chemistry and BSA was used for blocking of nonspecific binding sites of immunoelectrode. The BSA/anti-CYFRA-21-1/serine/nZrO_2/ITO electrode covers the whole physiological range including the lower secretion level of CYFRA-21-1 secreted in human saliva samples with linear detection range 0.01–29 ng mL^{-1}, sensitivity as 0.295 μA mL ng^{-1}, lower detection limit of 0.01 ng mL^{-1}, response time of 6 minutes and stability up to 45 days. Functionalization of nanostructured materials with non-hazardous serine molecules opens a new window in fabrication of biosensing platform as well as in fabrication of implantable biochip, drug delivery, gene delivery and in bioimaging systems.

Acknowledgements

We thank Prof Yogesh Singh, Vice Chancellor, Delhi Technological University, Delhi (India) for providing the research facilities. We thank Dr A. K. Dewan, Dr D. C. Dovel and Dr Birendra Kumar Yadav of Rajiv Gandhi Cancer Institute & Research Centre for valuable discussions. Suveen Kumar is thankful to DTU for the financial assistance. We thank Dr Laxman S. Meena, Institute of Genomics and Integrative Biology, Delhi, Dr Prabhakar Rai, Indian Institute of Technology-Kanpur for the TEM studies and Mr Sandeep Mishra, Central Facility, Delhi Technological University, Delhi for the XRD measurements.

References

1 A. Chen and S. Chatterjee, *Chem. Soc. Rev.*, 2013, **42**, 5425–5438.
2 M. A. Dobrovolskaia and S. E. McNeil, *Nat. Nanotechnol.*, 2007, **2**, 469–478.
3 V. Biju, *Chem. Soc. Rev.*, 2014, **43**, 744–764.
4 J. Conde, J. T. Dias, V. Grazú, M. Moros, P. V. Baptista and J. M. de la Fuente, *Front. Chem.*, 2014, 2.
5 S. Yadav, M. Mahato, R. Pathak, D. Jha, B. Kumar, S. R. Deka, H. K. Gautam and A. K. Sharma, *J. Mater. Chem. B*, 2014, **2**, 4848–4861.
6 S. R. Deka, S. Yadav, M. Mahato and A. K. Sharma, *Colloids Surf., B*, 2015, **135**, 150–157.
7 S. Yadav, V. Rai, M. Mahato, M. Singh, S. Rekha Deka and A. Kumar Sharma, *Curr. Top. Med. Chem.*, 2015, **15**, 1227–1235.
8 S. Kumar, S. Kumar, S. Tiwari, S. Srivastava, M. Srivastava, B. K. Yadav, S. Kumar, T. T. Tran, A. K. Dewan and A. Mulchandani, *Adv. Sci.*, 2015, **2**(8), 1500048.
9 S. Kumar, J. G. Sharma, S. Maji and B. D. Malhotra, *Biosens. Bioelectron.*\, 2016, **78**, 497–504.
10 S. Kumar, J. Singh, V. Agrawal, M. Ahamad and B. Malhotra, *Anal. Methods*, 2011, **3**, 2237–2245.
11 S. Kumar, S. Kumar, S. Srivastava, B. K. Yadav, S. H. Lee, J. G. Sharma, D. C. Doval and B. D. Malhotra, *Biosens. Bioelectron.*, 2015, **73**, 114–122.
12 S. K. Vashist, E. Lam, S. Hrapovic, K. B. Male and J. H. Luong, *Chem. Rev.*, 2014, **114**, 11083–11130.
13 V. K. Hsiao, J. R. Waldeisen, Y. Zheng, P. F. Lloyd, T. J. Bunning and T. J. Huang, *J. Mater. Chem.*, 2007, **17**, 4896–4901.
14 N. Nath and A. Chilkoti, *Anal. Chem.*, 2002, **74**, 504–509.
15 M. Pita, J. M. Abad, C. Vaz-Dominguez, C. Briones, E. Mateo-Martí, J. A. Martín-Gago, M. del Puerto Morales and V. M. Fernández, *J. Colloid Interface Sci.*, 2008, **321**, 484–492.
16 K. E. Sapsford, W. R. Algar, L. Berti, K. B. Gemmill, B. J. Casey, E. Oh, M. H. Stewart and I. L. Medintz, *Chem. Rev.*, 2013, **113**, 1904–2074.
17 A. Meister, *Biochemistry of the amino acids*, Elsevier, 2012.

18 A. White, P. Handler, E. Smith and D. Stetten Jr, *Principles of Biochemistry*, 1959.
19 O. Kujan, A. M. Glenny, R. Oliver, N. Thakker and P. Sloan, *The Cochrane Library*, 2006.
20 M. V. Gonzalez, M. L. Artimez, L. Rodrigo, C. López-Larrea, M. Menendez, V. Alvarez, R. Perez, M. Fresno, M. Perez and A. Sampedro, *J. Clin. Pathol.*, 1997, **50**, 212–217.
21 M. W. Lingen, J. R. Kalmar, T. Karrison and P. M. Speight, *Oral Oncol.*, 2008, **44**, 10–22.
22 L. L. Patton, J. B. Epstein and A. R. Kerr, *J. Am. Dent. Assoc.*, 2008, **139**, 896–905.
23 D. Rosenberg and S. Cretin, *Oral Surg., Oral Med., Oral Pathol.*, 1989, **67**, 621–627.
24 A. J. Bandodkar and J. Wang, *Trends Biotechnol.*, 2014, **32**, 363–371.
25 R. Malhotra, V. Patel, J. P. Vaqué, J. S. Gutkind and J. F. Rusling, *Anal. Chem.*, 2010, **82**, 3118–3123.
26 V. Pickering, R. C. Jordan and B. L. Schmidt, *Oral Oncol.*, 2007, **43**, 37–41.
27 R. Nagler, G. Bahar, T. Shpitzer and R. Feinmesser, *Clin. Cancer Res.*, 2006, **12**, 3979–3984.
28 K. Rajkumar, R. Ramya, G. Nandhini, P. Rajashree, A. Ramesh Kumar and S. Nirmala Anandan, *Oral Dis.*, 2015, **21**, 90–96.
29 T. Li and M. Yang, *Sens. Actuators, B*, 2011, **158**, 361–365.
30 J.-H. Wang, B. Wang, Q. Liu, Q. Li, H. Huang, L. Song, T.-Y. Sun, H. Wang, X.-F. Yu and C. Li, *Biomaterials*, 2013, **34**, 4274–4283.
31 C.-Y. Yang, E. Brooks, Y. Li, P. Denny, C.-M. Ho, F. Qi, W. Shi, L. Wolinsky, B. Wu and D. T. Wong, *Lab Chip*, 2005, **5**, 1017–1023.
32 M. Choudhary, P. Yadav, A. Singh, S. Kaur, J. Ramirez-Vick, P. Chandra, K. Arora and S. P. Singh, *Electroanalysis*, 2016, **28**, 1–11.
33 J. Jose, P. Sunil, R. Madhavan Nirmal and S. S. Varghese, *J. Oral Maxillofac. Pathol.*, 2013, 4.
34 D. L. Pavia, G. M. Lampman, G. S. Kriz and J. A. Vyvyan, *Introduction to spectroscopy*, Cengage Learning, 2008.
35 G. Sumana, M. Das, S. Srivastava and B. Malhotra, *Thin Solid Films*, 2010, **519**, 1187–1191.
36 D. Pavia, G. Lampman, G. Kriz and J. Vyvyan, *Introduction to spectroscopy*, Cengage Learning, 2008.
37 G. Liu and Y. Lin, *Anal. Chem.*, 2005, **77**, 5894–5901.
38 A. Vasudev, A. Kaushik and S. Bhansali, *Biosens. Bioelectron.*, 2013, **39**, 300–305.
39 A. Kaushik, P. R. Solanki, M. Pandey, S. Ahmad and B. D. Malhotra, *Appl. Phys. Lett.*, 2009, **95**, 173703.
40 J. Okuno, K. Maehashi, K. Kerman, Y. Takamura, K. Matsumoto and E. Tamiya, *Biosens. Bioelectron.*, 2007, **22**, 2377–2381.
41 Y. Wei, C. Gao, F.-L. Meng, H.-H. Li, L. Wang, J.-H. Liu and X.-J. Huang, *J. Phys. Chem. C*, 2011, **116**, 1034–1041.
42 C. J. Liu, S. Y. Kao, H. F. Tu, M. M. Tsai, K. W. Chang and S. C. Lin, *Oral Dis.*, 2010, **16**, 360–364.
43 S. Kumar, S. Kumar, S. Tiwari, S. Augustine, S. Srivastava, B. K. Yadav and B. D. Malhotra, *Sens. Actuators, B*, 2016, **235**, 1–10.